Magneto-Active Elastomer Filter for Tactile Sensing Augmentation through Online Adaptive Stiffening

Leone Costi[1], Arturo Tagliabue[2], Perla Maiolino,[3] Frank Clemens [2], Fumiya Iida[1]

***Abstract*—The mechanical properties of a sensor strongly affect its tactile sensing capabilities. The role of morphology and stiffness on the quality of the tactile data has already been the subject of several studies, which focus mainly on static sensor designs and design methodologies. However, static designs always come with trade-offs: considering stiffness, soft compliant sensors ensure a better contact, but at the price of mechanically filtering and altering the detected signal. Conversely, online adaptable filters can tune their characteristics, becoming softer or stiffer when needed. We propose a magneto-active elastomer filter which, when placed on top of the tactile unit, allows the sensor to change its stiffness on demand. We showcase the advantages provided by online stiffening adaptation in terms of information gained and data structure. Moreover, we illustrate how adaptive stiffening influences classification, using 9 standard machine learning algorithms, and how adaptive stiffening can increase the classification accuracy up to 34% with respect to static stiffness control.**

***Index Terms*—Force and Tactile Sensing, Soft Sensors and Actuators, Biologically-Inspired Robots.**

I. Introduction

The mechanical characteristics of any given structure (e.g. its stiffness) greatly affect and alter the capability to sense and process tactile information [1], [2]. Biological systems show us that adapting the sensors' mechanical characteristics to the environment is fundamental to achieve adequate sensitivity and high resolution. Nature has developed task-specific sensing networks for millions of years [3], developing sensors composed of different receptors, with varying morphology, spatial distribution, and density, perfectly tuned to achieve the best possible performance for the given task [4], [5]. Nevertheless, the complexity and the scale used by nature are still out of technology's reach, making morphing and adapting sensors very difficult to obtain [6].

Previously, researchers in this field have focused on the effect of different morphology designs, investigating the maximization of the information gain [7], the role of redundancy [8], sensitivity amplification [9], and task-specific optimization [10]. Moreover, there has been a considerable amount of studies on the relationship between the morphology of the sensor and the action for perception [11]–[13]. From these studies, it emerges the importance of the sensor's mechanical characteristics in action-based perception [14] and the trade-offs offered by a static structural design. Considering the sensor's stiffness as an example, softer interfaces offer more compliance [15]–[18] and more adhesion onto the object of interest [19], [20], thus increasing the contact area and the quality of tactile information. At the same time, a soft layer between sensor and object behaves as a 'mechanical low-pass filter', changing and perturbating the stimulus before it reaches the sensing elements [21]. The presence of such a trade-off is intrinsic in the nature of a static morphology that cannot be tuned online, thus being ideal for a specific task, but lacking generalization.

The natural solution to avoid the aforementioned problem is the implementation of online morphing filters. So far, there have only been a limited number of attempts due to the technological demanding challenge of such devices. Noticeable examples include the usage of hot melt adhesive to change the sensor morphology [22] and of liquid sensors able to tune their sensitivity and dynamic range [23]. A rather successful attempt has been made by *Hughes, Scimeca, et al.* [24]: they use granular jamming to change the morphology of a tactile sensor and prove that the ability to change the sensor's morphology online produces enhanced classification performance. However, for the system to work, it is needed an external pump and a set of known morphing stands that are used to change the filter's morphology. As a result, the change between filter configurations is very slow and relies on external devices.

The aim of this work is to implement a fast, robust, and compact mechanism able to rapidly change the sensor's stiffness online, to improve tactile information-based object classification. Moreover, we plan to achieve such an aim without the need for external devices or known surfaces, like in previous works, but only with a sensorized UR5 robotic arm (*Universal Robots*). To do so, we plan to use a magneto-active elastomer (MAE) as a soft interface between the tactile sensor and the object of interest. We are able to tune the MAE's stiffness almost instantly thanks to an electromagnet placed between the sensor and the UR5. We will prove that selectively increasing the stiffness, after the first contact is made, ensures a good fit and produces higher quality tactile data, when compared to maintaining the same stiffness throughout the whole touching process.

We will implement 3 different stiffening strategies on a set of 12 objects varying stiffness, roughness, and shape. Moreover, the tactile data obtained with online stiffness adap-

Manuscript received: October 11, 2021; Revised: January 11, 2022; Accepted: February 28, 2022.

This paper was recommended for publication by Editor Cecilia Laschi upon evaluation of the Associate Editor and Reviewers' comments.

[1] The Bio-Inspired Robotics Lab, Department of Engineering, University of Cambridge, UK.

[2] Swiss Federal Laboratories for Materials Science and Technology, Switzerland.

[3]Oxford Robotics Institute, University of Oxford, UK.

Digital Object Identifier (DOI): see top of this page.

tation will be compared with the ones of the two static configurations, low and high stiffness. First, the data will be characterized in terms of variance retention and clustering behaviors, then they will be used as input for 9 standard machine learning classification algorithms to show that adapting the filter's stiffness online can ultimately result in higher classification accuracy, up to 34%.

In the remainder of the paper, we will describe the manufacturing of the MAE and the implementation of the overall sensing system, as well as the implementation of the testing bench, in Section II, followed by the results in Section III and the conclusion and final remarks in Section IV.

II. Materials and Methods

A. System overview

The entire sensing system is designed to fit on the end-effector of a UR5 robotic arm and it is composed of an electromagnet, a tactile sensor, and the MAE (see Fig. 1). When the magnet is activated, the MAE changes its visco-elastic properties. In this study, we aim to exploit the increase of compression modulus induced by the magnetic field, thus differentiating between a softer configuration when the magnet is off, and a stiffer one when the magnet is on.

The magnet (*RS PRO magnet 791-7567, RS Components*) is connected to the end-effector with screws and powered via cable from the $24\ V$ tool output of the UR5. The dimensions of the magnet are a trade-off between the magnetic strength required by the MAE and the volumetric and weight constraints imposed by the UR5's end-effector: we selected the biggest magnet that can be carried as payload by the manipulator. This configuration allows us to avoid external devices, thus increasing the operating frequency of the manipulator up to $125\ Hz$. The tactile sensor is a circular capacitive sensor disk that has 50 'taxels' providing high sensitivity and spatial distribution over the surface of the sensor, glued on top of the magnet. The sensor provides measurement with a resolution of 16 bits corresponding to a variation of capacitance proportional to the pressure acting on top of it. Details of the specific sensor and its fabrication have been previously reported [25].

The MAE filter is a $3\ mm$ thick layer obtained by placing 4 $27 \times 27 \times 3\ mm$ MAE samples on top of the tactile sensor. The adhesion is obtained by applying with a brush a thin layer of Dragon-skin 20 (*Smooth-On, Inc.*) on the sensor, before placing the filter, and allow it to cure before using the system. The MAE is composed of a matrix of silicone and inner carbonyl iron particles (CIP). Further details about the fabrication process are discussed in Section II-B. During the experimental trials, the system is placed above the selected object, and then the sensing action is performed in 2 steps: approaching phase and touch phase. First, the end-effector is moved down until the sensor is able to successfully detect that a contact has been made, and later a 'rubbing motion' on the xy plane is performed (see Section II-C).

B. MAE manufacturing

For the elastomer matrix, Ecoflex 00-10 polymer (*Smooth-On, Inc.*), with a specific gravity of $1.04\ g/cm^3$ and a shore hardness below 1, was used. As the magnetoactive filler, CIP with a mean particle size of 1.9 µm (*BASF, Ludwigshafen, Germany*) were used (see Fig. 2*a* and 2*b*). SolidWorks was used to design appropriate molds for casting the samples with a size of $27 \times 27 \times 1$, $27 \times 27 \times 3$, and $27 \times 27 \times 5\ mm^3$, respectively. These molds were 3D-printed using CraftFilament PLA (*CraftWare, Hungary*).

To achieve a silicone with $30\ vol.\%$ CIP, the magnetic particles were pre-mixed with Ecoflex 00-10 (1:1 ratio monomer and hardener) for 1 minute using a manual stirrer. To lower the viscosity, $10\ mL$ of acetone ($7.9\ g$) were added to $237.7\ g$ MAE before final mixing on a 3-roller mill (*Exakt, type 80 S*). Before pouring the liquid into the mold, an anti-sticking spray was used. The liquid MAE was poured into the mold and any excess material was removed by tape casting using a doctor blade. In the last step, the material was heated in an oven at $60°C$ to speed up the solidification process, avoiding unnecessary sedimentation of CIP in the matrix. Both the low and high stiffness states have been characterized with compression tests (see Fig. 2*c*): the filter has been tested with a $500\ N$ load cell (*2580-500N, Instron*) on a screw driven compression testing machine (*5584, Instron*) with a single

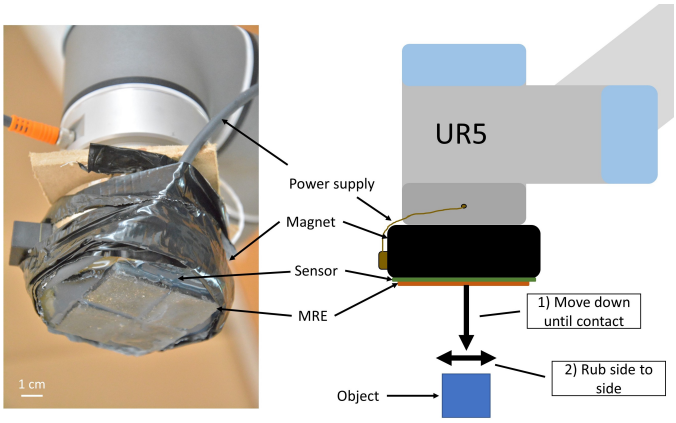

Fig. 1. On the left, implementation of the MAE filter on the tactile sensor at the end-effector of the UR5. On the right, Schematics of the system and the executed task.

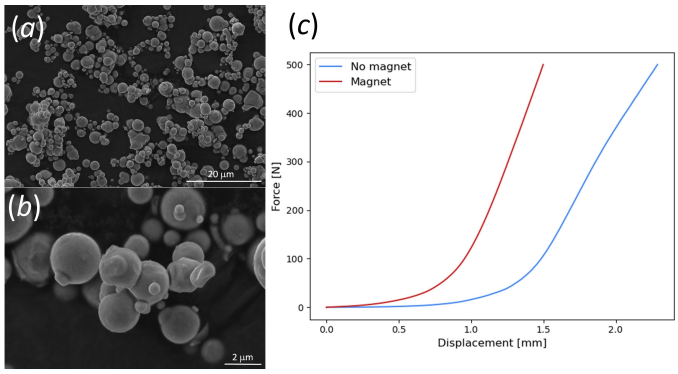

Fig. 2. On the left, scanning electron microscopy of carbonyl iron particles at 20 μm (*a*) and 2 μm (*b*). On the right (*c*), compression tests' result of the MAE filter with and without the magnetic field.

cycle compression at 1 mm/min, to limit the effect of the MAE's viscosity.

C. Experimental protocol

In order to test the effect of online filter stiffening on discrimination tasks, we collect tactile data on a set of 12 objects with different shapes, roughness, and stiffness, in 3 different stiffening strategies: magnet off (MO), magnet before contact (MBC), and magnet after contact (MAC). On one hand, MO and MBC represent static stiffening strategies, where the stiffness of the material is constant during the whole touching process, being the magnet always switched off in MO and on in MBC. On the other, MAC is an online adaptive stiffening strategy, because the MAE filter is kept in its low stiffness state for the approaching phase, and the magnet is turned on after the contact.

The approaching phase consists of the lowering of the end-effector to achieve contact with the object of interest. For each object to touch, the end-effector is controlled to move normally downward until a touch event is detected by the capacitive tactile sensor at its extremity. The touch event consists of a raise, in any of the 50 taxels, by more than 5% of their reading range. Note that, since the approaching phase is terminated after reaching a pressure threshold, the stiffness of the MAE directly affects the level of interaction with the object. In MO and MAC, the filter is softer while approaching the object, achieving a deeper interaction, whereas in MBC the filter is stiffer from the start of the trial, leading to less compliance upon contact and earlier stop of the approaching phase, thus having a more shallow interaction. The touch phase consists of a controlled 5 seconds interaction between the sensorized end-effector and the object under trial. After contact is detected, the robot proceeds to perform a 'rubbing motion', by moving 3 mm diagonally in the xy plane for 5 s. In the touch phase, the sensor is sampled at 50 Hz. We thus retrieve a total of 250 tactile images for each experiment, each containing responses from 50 different taxels. This brings the dimensionality of each tactile experiment to a 12,500-dimensional vector.

The set of objects used for the experiments consists of 12 objects with different mechanical characteristics: 2 different levels of roughness, smooth and rough, 2 different object's shapes, square and round, and 3 different stiffness levels, obtained by using different manufacturing materials (see Fig. 3). The 3 materials used to manufacture the test objects are PLA, Dragon-skin 20, and Ecoflex 00-10: non-elastomeric PLA objects are directly 3D printed, whereas elastomeric silicone-based ones are the result of silicone casting in 3D printed PLA molds. Concerning the shape, the squares are fabricated as 20 mm edge cubes and the rounds are 20 mm diameter and 10 mm height cylinders with 20 mm diameter half-spheres on top. Finally, the rough objects are made ridged by adding 1 mm deep and 1 mm wide grooves on the object's top surface, at a distance of 1 mm.

Every object is subject to 50 trials for each of the 3 stiffening strategies, for a total of 150 trials per object and 1800 overall trials. Fig. 4 illustrates the work-flow of a single trial. The trials are executed in random order without replacement. This also results in a pulsed activation of the magnet, given the random order of trials with and without the magnetic field, rather than a continuous one. Avoiding continuous activation of the magnet strongly reduces a potential increase in temperature, which could change the MAE visco-elastic properties. The outcomes of the proposed protocol are 3 distinct datasets (MO, MBC, and MAC), that will be analyzed and compared in Section III.

D. Data processing

Given the amount of data produced by the experimental trials and the high number of dimensions of each data point, we decided to implement a dimensionality reduction technique and to verify if there are any clustering behaviors for data points belonging to the same object.

First, we opted to apply principal component analysis (PCA) to reduce the number of dimensions of our dataset. This is used to strongly reduce the initial number of dimensions, 12,500, to a pre-selected number of principal components, where p_i is the i^{th} principal component retained [26]. Then, we evaluate the information loss by analyzing what fraction of the original data variance is retained as a function of the number of considered principal components.

Next, we analyze how structured are the acquired data. Ideally, a good data structure has a low intra-class distance among data points belonging to the same object, and a high inter-class distance among different objects. For the purpose of this work, each object corresponds to a different class, for a total of 12 classes. A metric that can be used to have a first approximation of the structure's quality is the Silhouette score [27]. Such a metric has already been implemented in tactile information-based discrimination tasks [28] and can be computed as follows:

$$s(i) = \frac{b(i) - a(i)}{max(a(i), b(i))} \tag{1}$$

where $a(i)$ is the mean intra-class distance and $b(i)$ is the mean nearest-class distance for the object i. To summarize the results, we will refer to a Silhouette score s as the mean of the scores of individual classes $s(i)$ for $i = 1, .., 12$. The score s can thus assume values between -1 and 1 included, where higher values correspond to a better defined data structure, which may lead to a more accurate classification.

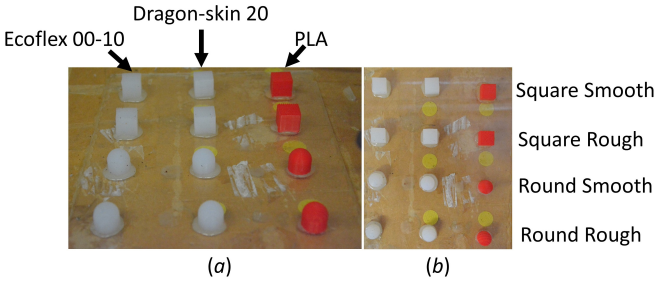

Fig. 3. (A) Side view and (B) top view of different dummies used for the recognition task. From left to right: Ecoflex 00-10, Dragon-skin 20, and PLA. From top to bottom: Smooth Square, Rough Square, Smooth Round, Rough Round.

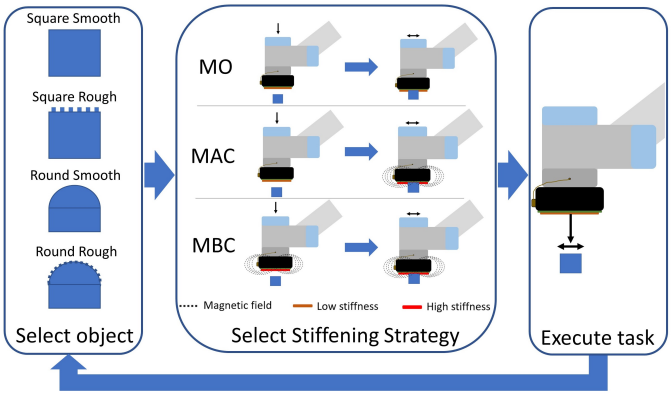

Fig. 4. Work-flow of a single trial during data collection. First, the object of interest is selected among the 12 possible options: 4 combinations of shape and roughness for each of the 3 levels of stiffness. Next, the stiffening strategy for the current trial is selected: in MO the MAE is kept in its low stiffness state for the entire trial, in MBC it is kept stiff for the entire trial, and in MAC it is initially off, and then it is turned on after the contact with the object is detected. Finally, the task is executed and the tactile data are saved in the respective dataset (MO, MBC or MAC).

E. Classification

In order to further analyze the quality of the tactile information, we compare the performance of several machine learning algorithms (MLAs) while working on the 3 datasets. We decided to select 9 standard MLAs: Feed Forward Neural Network [29], QDA [30], Linear SVM [31], RBF SVM [32], Nearest Neighbors [33], Gaussian Process [34], Decision Tree [35], Random Forest [36], and Naive Baise [37]. The choice behind such a high number of different algorithms is that we do not want our conclusion to be biased by a specific feature of a single classifier, thus by considering different ones we aim to highlight the difference in the quality of the provided data over the intrinsic difference among them. We assume that better data would lead to a better classification in the majority of the cases. All the classifiers are implemented using Python 3.8 built-in functions with default parameters and trained on the same 3 datasets (MO, MBC, and MAC).

III. Results

This Section elaborates on the results obtained using the tactile data generated following the experimental protocol described in Section II-C, with primarily focus on the performance difference between the 3 datasets (MO, MBC, and MAC), corresponding to the 3 stiffening strategies.

A. Filter response

To show how the change in stiffness affects the tactile sensing, Fig. 5 illustrates the raw tactile signal picked up in the 3 different stiffening strategies for all 12 objects. The images are taken after 2.5 s of the touch phase, performed as described in Section II-C. By comparing images belonging to the same object, it is clear that the change in stiffness does not radically change the overall response of the sensor, but rather promotes some noticeable changes in the contact area, where the interaction with the object is detected. It is clear that changing the stiffness alters the tactile information because it alters the mechanical interaction between object and sensor during the touch phase.

B. Data processing

In order to reduce the dimensionality of the data points, a PCA was applied to the dataset. The main metric to assess the goodness of the PCA is the percentage of data variance preserved as a function of how many principal components are retained. At the same time, the Silhouette score, as shown in Section II-D, is a good metric to understand the correct clustering of data points. Fig. 6 shows the results in terms of PCA variance retention and Silhouette score as a function of the principal components and of the stiffening strategy employed. More in detail, the Silhouette score is computed for different values of retained dimensions in order to avoid any bias caused by the dimensionality reduction's choice.

Firstly, it can be noticed that the MAC dataset can cumulatively retain more information than the other 2: considering the number of needed components to achieve 80% of the initial variance, MAC only needs 7, against the 8 of MBC and the 9 of MO. Moreover, the first component is able to retain 5% and 15% more variance than its counterparts, MBC and MO, respectively. Next, MAC also showcases a higher Silhouette score for any number of considered dimensions, having the bigger difference between 4 and 9. Those results prove that changing the stiffness of the filter between the approaching and touch phase allows better variance retention when applying PCA and produces more structured data.

To further analyze the data structure, Fig. 7 illustrates the 2D plots of the data points according to the first 2 principal components, one for each stiffening strategy. Here, it can be appreciated how MAC contributes to a better separation of the data by decreasing the intra-class distance. In fact, even if it has a limited effect on inter-class distance, it successfully manages to bring closer data points belonging to the same class, or object, especially in the central most crowded portion of the plots. This visualization of the tactile data clarifies the mechanism causing MAC's higher Silhouette score.

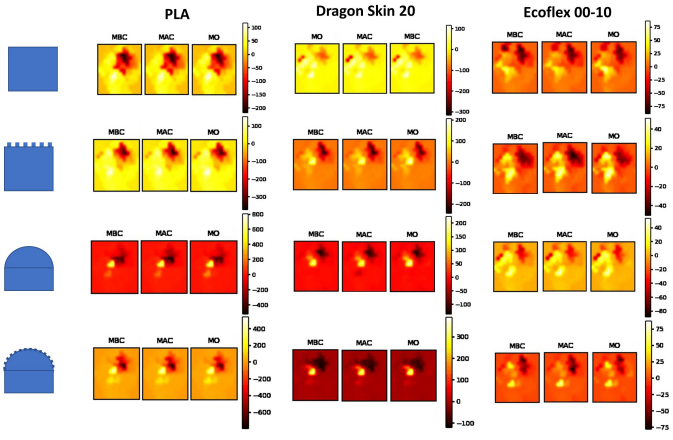

Fig. 5. Raw tactile sensor activation after 2.5 seconds from the beginning of the touch experiment. Brighter colors correspond to higher sensor values.

C. Classification

Finally, we test how the higher variance retention and the better structure of the data affect the classification performance. To do so, every object is considered a different class, thus we have 12 classes and a random choice performance of 8.3%. We selected accuracy as a performance metric because the datasets are balanced, with exactly 50 data points per object for each stiffening strategy. Fig. 8 shows the performance of the 9 MLAs used to test the datasets as a function of the stiffening strategy and the number of retained principal components.

MAC is shown to achieve a better performance than the other 2 datasets by a large margin: it scores an overall better average accuracy in 8 classifiers, leaving out only Forward Neural Network. The largest difference is registered in RBF SVM and Gaussian Process, where the accuracy increment reaches a maximum of 34%. Moreover, MAC clearly provides a better classification than MBC in more than half of the classifiers, even if they both use the stiffer configuration during the touch phase. This can be explained by the difference in interaction with the objects: in MAC, the low stiffness approaching phase allows the filter to better adapt its morphology to the object, obtaining a better contact, whereas MBC is characterized by a stiff MAE throughout both phases, resulting in a lower interaction with the object. Hence, the results suggest that 2 factors influence the quality of the tactile data: the filter's stiffness during the touch phase and the level of interaction, which is determined by the filter's stiffness during the approaching phase. Depending on the classification algorithm, the relative importance of those 2 factors can greatly change: as an example, Random Forest seems to be affected mostly by the touch phase filter's stiffness, with similar performance for MBC and MAC, whereas RBF SVM strongly increases its accuracy only when both factors are present, in MAC.

IV. Conclusion

In this work, we proposed an MAE online adaptive filter, able to change its stiffness on demand. Moreover, unlikely other adaptive filters present in state-of-the-art literature, our system can easily fit on top of the end-effector of a robotic arm, without the need of external devices nor additional control boards, and ensures a rapid switch between the filter's possible configurations.

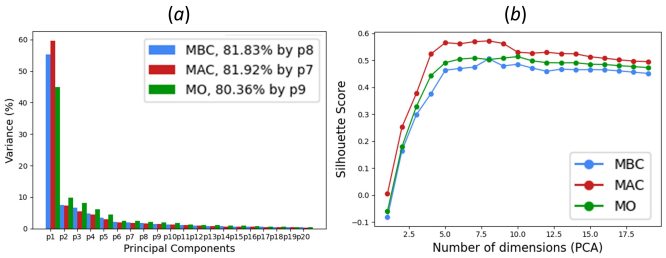

Fig. 6. The variance retention of the principle components (a) and the silhouette score for increasing number of dimensions (b), for each stiffening strategy. The 3 datsets (M0, MBC and MAC) have been obtained through the experimental protocol in Section II-C.

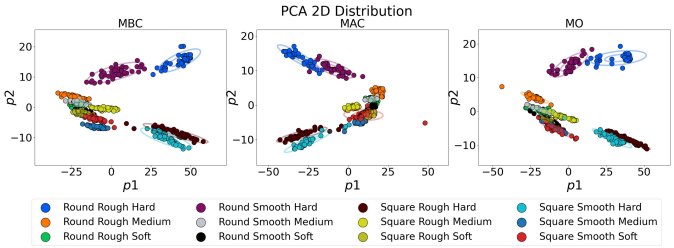

Fig. 7. PCA 2D projections of the sensor response. Each figure is generated via touch experiments with a different stiffening strategy (see Section II-C). The ellipses are drawn at 1 standard deviation and 3 standard deviations.

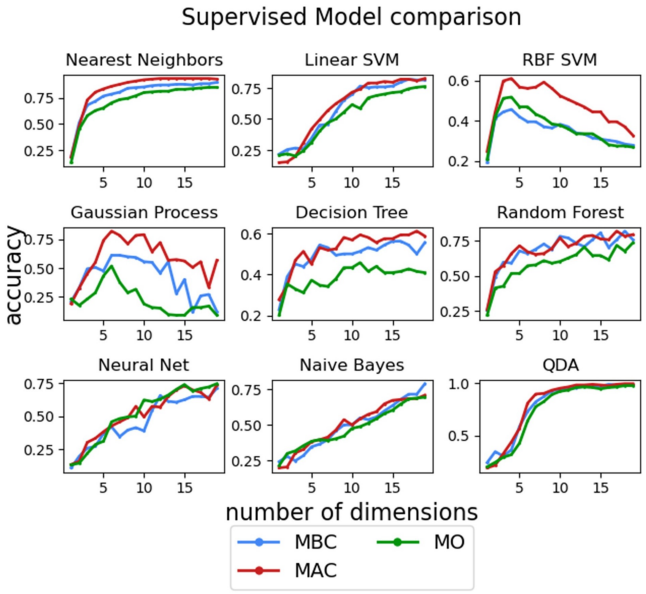

Fig. 8. Accuracy when performing classification of the different objects using the 9 different classifiers a function of the PCA dimensions. The 3 datasets (MO, MBC, and MAC) have been obtained according to Section II-C.

To test the performance of the filter we acquired data from a set of 12 objects of variable shape, roughness, and stiffness, using 3 different stiffening strategies: magnet off, magnet before contact, and magnet after contact. A total of 1800 trials have been executed in a random order to minimize time-variant bias and possible temperature increase due to continuous magnet operation. Using the PCA variance retention and the Silhouette score, we demonstrated that online stiffness adaptation successfully produces higher quality tactile data, showcasing both greater variance retention and a more separable data structure. Generally, online adaptive stiffening produces more structured tactile data when compared to constant stiffness, either low or high. Moreover, we prove that online stiffness adaptation's data produce increased accuracy when using 9 different standard machine learning classification algorithms, up to 34%.

Overall, we showcased how to compactly and rapidly achieve online stiffness adaptation and its potential. The ability to tune the compliance of the tactile sensor at the right

moment, instead of pre-selecting it, can affect substantially the quality of the collected data, and in turn increase the performance of classification algorithms. However, we acknowledge that our work is limited to stiffness adaptation, and does not cover morphological changes, due to the simple geometry of the MAE filter. Moreover, the magnet's positioning is not ideal in order to maximize the compression modulus increase: the field loops around the magnet, thus its magnitude inside the material rapidly decreases when moving away from the magnet itself. Future work could also include computational modelling of the magnetic field inside the material and modulating it so to sweep along a stiffness' range, instead of two discrete states. Lastly, we believe that online adaptive stiffening is not limited to active touch, but can be effective also during passive touch, since it only depends on the relative motion between sensor and object, and we endorse further studies on this topic.

ACKNOWLEDGMENT

This work was supported by the SMART project, European Union's Horizon 2020 research and innovation under the Marie Sklodowska-Curie (grant agreement ID 860108).

REFERENCES

[1] L. Scimeca, P. Maiolino, and F. Iida, "Soft morphological processing of tactile stimuli for autonomous category formation," in *2018 IEEE International Conference on Soft Robotics (RoboSoft)*. IEEE, 2018, pp. 356–361.

[2] J. Hughes and F. Iida, "Localized differential sensing of soft deformable surfaces," in *2017 IEEE International Conference on Robotics and Automation (ICRA)*. IEEE, 2017, pp. 4959–4964.

[3] A. E. Rawlings, J. P. Bramble, and S. S. Staniland, "Innovation through imitation: Biomimetic, bioinspired and biokleptic research," *Soft Matter*, vol. 8, no. 25, pp. 6675–6679, 2012.

[4] A. B. Vallbo, R. S. Johansson *et al.*, "Properties of cutaneous mechanoreceptors in the human hand related to touch sensation," *Hum neurobiol*, vol. 3, no. 1, pp. 3–14, 1984.

[5] T. Maeno, K. Kobayashi, and N. Yamazaki, "Relationship between the structure of human finger tissue and the location of tactile receptors," *JSME International Journal Series C Mechanical Systems, Machine Elements and Manufacturing*, vol. 41, no. 1, pp. 94–100, 1998.

[6] F. Iida and S. G. Nurzaman, "Adaptation of sensor morphology: an integrative view of perception from biologically inspired robotics perspective," *Interface focus*, vol. 6, no. 4, p. 20160016, 2016.

[7] T. G. Thuruthel, J. Hughes, and F. Iida, "Joint entropy-based morphology optimization of soft strain sensor networks for functional robustness," *IEEE Sensors Journal*, vol. 20, no. 18, pp. 10 801–10 810, 2020.

[8] L. Costi, T. G. Thuruthel, and F. Iida, "Topological Study on the Design of Soft Strain Sensors for Simultaneous Multi-point Contact Localization," pp. 555–558, 2021.

[9] M. Fend, R. Abt, M. Diefenbacher, S. Bovet, and M. Krafft, "Morphology and learning-a case study on whiskers," in *Proc. 8th Int. Conf. on the Simulation of Adaptive Behavior*, 2004, pp. 114–122.

[10] Q. Qi, S. Hirai *et al.*, "Wrinkled soft sensor with variable afferent morphology," *IEEE Robotics and Automation Letters*, vol. 4, no. 2, pp. 1908–1915, 2019.

[11] I. Huang, J. Liu, and R. Bajcsy, "A depth camera-based soft fingertip device for contact region estimation and perception-action coupling," in *2019 International Conference on Robotics and Automation (ICRA)*. IEEE, 2019, pp. 8443–8449.

[12] L. Scimeca, P. Maiolino, and F. Iida, "Efficient bayesian exploration for soft morphology-action co-optimization," in *2020 3rd IEEE International Conference on Soft Robotics (RoboSoft)*. IEEE, 2020, pp. 639–644.

[13] L. Scimeca, J. Hughes, and F. Iida, "Action augmentation of tactile perception for soft-body palpation," *Soft robotics*, 2021.

[14] J. E. Bernth, V. A. Ho, and H. Liu, "Morphological computation in haptic sensation and interaction: from nature to robotics," *Advanced Robotics*, vol. 32, no. 7, pp. 340–362, 2018.

[15] E. Brown, N. Rodenberg, J. Amend, A. Mozeika, E. Steltz, M. R. Zakin, H. Lipson, and H. M. Jaeger, "Universal robotic gripper based on the jamming of granular material," *Proceedings of the National Academy of Sciences*, vol. 107, no. 44, pp. 18 809–18 814, 2010.

[16] L. Margheri, C. Laschi, and B. Mazzolai, "Soft robotic arm inspired by the octopus: I. from biological functions to artificial requirements," *Bioinspiration & biomimetics*, vol. 7, no. 2, p. 025004, 2012.

[17] R. Pfeifer, F. Iida, and M. Lungarella, "Cognition from the bottom up: on biological inspiration, body morphology, and soft materials," *Trends in cognitive sciences*, vol. 18, no. 8, pp. 404–413, 2014.

[18] A. D. Hinitt, J. Rossiter, and A. T. Conn, "Wormtip: An invertebrate inspired active tactile imaging pneumostat," in *Conference on Biomimetic and Biohybrid Systems*. Springer, 2015, pp. 38–49.

[19] H. X. Trinh, K. Shibuya *et al.*, "Theoretical foundation for design of friction-tunable soft finger with wrinkle's morphology," *IEEE Robotics and Automation Letters*, vol. 4, no. 4, pp. 4027–4034, 2019.

[20] Q. Qi *et al.*, "Wrinkled soft sensor with variable afferent morphology: Case of bending actuation," *IEEE Robotics and Automation Letters*, vol. 5, no. 3, pp. 4102–4109, 2020.

[21] M. Shimojo, "Mechanical filtering effect of elastic cover for tactile sensor," *IEEE Transactions on Robotics and Automation*, vol. 13, no. 1, pp. 128–132, 1997.

[22] S. G. Nurzaman, U. Culha, L. Brodbeck, L. Wang, and F. Iida, "Active sensing system with in situ adjustable sensor morphology," *PLoS One*, vol. 8, no. 12, p. e84090, 2013.

[23] K.-W. Liao, M. T. Hou, H. Fujita, and J. A. Yeh, "Liquid-based tactile sensing array with adjustable sensing range and sensitivity by using dielectric liquid," *Sensors and Actuators A: Physical*, vol. 231, pp. 15–20, 2015.

[24] J. Hughes, L. Scimeca, P. Maiolino, and F. Iida, "Online Morphological Adaptation for Tactile Sensing Augmentation," *Frontiers in Robotics and AI*, vol. 8, no. July, pp. 1–13, 2021.

[25] P. Maiolino, M. Maggiali, G. Cannata, G. Metta, and L. Natale, "A flexible and robust large scale capacitive tactile system for robots," *IEEE Sensors Journal*, vol. 13, no. 10, pp. 3910–3917, 2013.

[26] H. Abdi and L. J. Williams, "Principal component analysis," *Wiley interdisciplinary reviews: computational statistics*, vol. 2, no. 4, pp. 433–459, 2010.

[27] P. J. Rousseeuw, "Silhouettes: a graphical aid to the interpretation and validation of cluster analysis," *Journal of computational and applied mathematics*, vol. 20, pp. 53–65, 1987.

[28] L. Scimeca, P. Maiolino, E. Bray, and F. Iida, "Structuring of tactile sensory information for category formation in robotics palpation," *Autonomous Robots*, vol. 44, no. 8, pp. 1377–1393, 2020.

[29] D. E. Rumelhart, G. E. Hinton, and R. J. Williams, "Learning representations by back-propagating errors," *nature*, vol. 323, no. 6088, pp. 533–536, 1986.

[30] F. Pedregosa, G. Varoquaux, A. Gramfort, V. Michel, B. Thirion, O. Grisel, M. Blondel, P. Prettenhofer, R. Weiss, V. Dubourg, J. Vanderplas, A. Passos, D. Cournapeau, M. Brucher, M. Perrot, and E. Duchesnay, "Scikit-learn: Machine learning in Python," *Journal of Machine Learning Research*, vol. 12, pp. 2825–2830, 2011.

[31] E. Mayoraz and E. Alpaydin, "Support vector machines for multi-class classification," in *International Work-Conference on Artificial Neural Networks*. Springer, 1999, pp. 833–842.

[32] X.-f. Yan, H.-w. Ge, and Q.-s. Yan, "Svm with rbf kernel and its application research," *Computer Engineering and Design*, vol. 27, no. 11, pp. 1996–1997, 2006.

[33] J. Goldberger, G. E. Hinton, S. Roweis, and R. R. Salakhutdinov, "Neighbourhood components analysis," *Advances in neural information processing systems*, vol. 17, pp. 513–520, 2004.

[34] C. KI Williams, *Gaussian processes formachine learning*. Taylor & Francis Group, 2006.

[35] D. Steinberg and P. Colla, "Cart: classification and regression trees," *The top ten algorithms in data mining*, vol. 9, p. 179, 2009.

[36] A. Cutler, D. R. Cutler, and J. R. Stevens, "Random forests," in *Ensemble machine learning*. Springer, 2012, pp. 157–175.

[37] C. D. Manning, P. Raghavan, and H. Schutze, "Introduction to information retrieval?" *Ch*, vol. 20, pp. 405–416, 2008.